

# Supporting Information

Walter *et al.* 10.1073/pnas.0801001105

## SI Text

**Computational Methods.** **CP2K.** The geometry optimization and electronic structure calculation of the full isolated  $\text{Au}_{102}(\text{p-MBA})_{44}$  particle is performed by using a recently developed program package, CP2K (1, 2), that is based on the density-functional theory (DFT) of electronic structure. Central in this method is the use of two representations of the electron density: localized Gaussian and plane wave (GPW) basis sets. This kind of representation allows for an efficient treatment of the electrostatic interactions and leads to a scheme that is formally linearly scaling as a function of the system size. This is crucial for gold nanoparticles of this size because the standard DFT methods turned out to be extremely demanding in terms of both computing time and memory.

The valence electron-ion interaction is based on the norm-conserving and separable pseudopotentials of the analytical form derived by Goedecker, Teter, and Hutter (GTH) (3). We considered the following valence configurations:  $\text{Au}(5\text{d}^{10}6\text{s}^1)$ ,  $\text{C}(2\text{s}^22\text{p}^2)$ ,  $\text{H}(1\text{s})$ ,  $\text{O}(2\text{s}^22\text{p}^4)$ , and  $\text{S}(3\text{s}^23\text{p}^4)$ . The optimized pseudopotentials include scalar relativistic corrections via an averaged potential, and they improve the accuracy for Au considerably. For the Gaussian-based (localized) expansion of the Kohn-Sham orbitals we use a library of contracted m-DZVP basis sets (4), and the complementary plane wave basis set has a cut-off of 320 rydberg (Ry) for electron density (this equals 80 Ry for wave functions in standard plane wave schemes). The recently developed molecularly optimized m-DZVP functions result in highly accurate results with less computational cost as experienced with the traditional basis sets that are fitted to atomic properties. The generalized gradient-corrected approximation of Perdew, Burke, and Ernzerhof (PBE) is adopted for the exchange-correlation energy functional (5).

The DFT calculations start from the coordinates published from the experimental x-ray diffraction measurement (6). The experimental coordinates do not contain hydrogen atom positions in the *p*-MBA ligands, and these are generated separately. There are two classes of H atoms: (i) atoms attached to the aromatic C atoms, and (ii) atoms participating in the terminal hydroxyl groups. We can exclude the existence of hydrogens in the sulfur end (see discussion below). It is straightforward to add the first group of H atoms by using the standard C-H bond distance and C-C-H angles. For the terminal OH groups there are two oxygen atoms that can bind H covalently. The experimental data do not indicate a preferable oxygen for the H binding due to an averaging-out effect (no difference in the two bonds in the O-C-O unit). In that case we choose the H-binding oxygen randomly. The OH bond length as well as its orientation was fitted to the well known (calculated) values of carboxylic acids. The resulting geometry contains 220 H atoms in 44 *p*-MBA side groups, and the total number of atoms and valence electrons is 762 and 3,366, respectively. This adding scheme resulted in a system that had a neutral net charge. Finally, the system is placed in a cubic simulation box of 35 Å, which is large enough to separate periodic replica of the nanoparticle (the calculations were carried out with periodic boundary conditions).

The electronic structure is analyzed in three stages. In stage A, we analyze the experimental structure, and as expected, some undesirable effects can be observed in the projected density of states (P-DOS) as a result of some artificially short covalent bonds in the side groups (especially the C-O bonds). The next stage, B, consists of optimization of *all of the ligands* (Au atoms fixed). The effect of this optimization is reflected in P-DOS as

a reduced weight close to Fermi energy of the electron states that reside dominantly in the ligands. During this stage of the geometry optimization, only a minor change of the orientations of the ligands is observed. Our electronic structure analysis, presented in this article, is based on this optimization stage.

Parallel to the analysis of the electronic structure based on stage B described above, we have also optimized the  $\text{Au}_{79}$  core as well as releasing the 23 Au atoms in the Au-ligand layer, i.e., *all of the atoms* in the nanoparticle are made dynamic. As expected for the PBE functional, the Au-Au nearest-neighbor distances in the core expand slightly (by 2%) but no change in the symmetry, or a significant effect in the electronic density of states, is observed.

**GPAW.** The model compound  $\text{Au}_{102}(\text{SMe})_{44}$  (see *Comparison of CP2K and GPAW Results*. . . below), the  $\text{Au}_{39}(\text{PH}_3)_{14}\text{Cl}_6^-$  cluster, and the  $\text{Au}_{11}(\text{PH}_3)_7\text{Cl}_3$ ,  $\text{Au}_{11}(\text{PH}_3)_7(\text{SMe})_3$ , and  $\text{Au}_{13}(\text{PH}_3)_{10}\text{Cl}_2^{3+}$  clusters are optimized and analyzed by using a recently developed GPAW DFT software (<https://wiki.fysik.dtu.dk/gpaw>). Analyses of  $\text{Au}_{79}$  core,  $\text{Au}_{80}(\text{p-MBA})_2$ , and isolated *p*-MBA units are also performed using the GPAW code. Here, the projector augmented wave (PAW) method (7) has been implemented in a real space grid as described in ref. 8. In the PAW method the all-electron Kohn-Sham wave functions are divided into a smooth part and a highly oscillatory part. The oscillatory part is localized inside an atom-centered sphere, where it can be expanded effectively in an atom-centered orbital basis function. The PAW method solves the equivalent Schrödinger equation for a transformed auxiliary wave function that is suitably smooth in the atom-centered sphere. Using this transformation, it is possible then to take advantage of coarse grids while the all-electron density is still accessible.

The inner electrons were treated in the frozen core approximation, leaving the  $\text{Au}(5\text{d}^{10}6\text{s}^1)$ ,  $\text{C}(2\text{s}^22\text{p}^2)$ ,  $\text{Cl}(3\text{s}^23\text{p}^5)$ ,  $\text{H}(1\text{s})$ ,  $\text{O}(2\text{s}^22\text{p}^4)$ ,  $\text{P}(3\text{s}^23\text{p}^5)$ , and  $\text{S}(3\text{s}^23\text{p}^4)$  as valence electrons. The PAW setup for gold includes scalar-relativistic corrections. Convergence was achieved in a grid spacing of 0.1 Å for the smooth electron density, corresponding to a 69-Ry plane wave cut-off. The exchange-correlation energy and potential were evaluated using the generalized gradient approximation as derived by Perdew, Burke, and Ernzerhof (PBE-functional) (5).

## Comparison of CP2K and GPAW Results for the Model Cluster

**$\text{Au}_{102}(\text{SMe})_{44}$ .** As a cross-check of the density-functional results from the CP2K method for the  $\text{Au}_{102}(\text{p-MBA})_{44}$  cluster we considered a somewhat smaller system  $\text{Au}_{102}(\text{SMe})_{44}$ , where the *p*-MBA ligands are replaced by methylthiolates (the positions of the Au atoms and S atoms are taken from the experimental data and locally optimized methyl units are attached to each sulfur). This system has 1,694 valence electrons. We solved the electronic structure of this cluster both from the CP2K and from the GPAW method. Comparison of HOMO-LUMO gaps, density of states, or angular momentum character of the states around the HOMO-LUMO gap shows that these two methods give virtually identical description of the electronic structure of the  $\text{Au}_{102}(\text{SMe})_{44}$  model cluster.

## The Angular Momentum Analysis of Kohn-Sham Wave Functions.

Taking the center for the expansion to be the center of mass of the cluster we calculate the coefficients

$$c_l(R_0) = \sum_m \int_0^{R_0} r^2 dr |\psi_{nlm}(r)|^2$$

where

$$\psi_{nlm}(r) = \int d\hat{\mathbf{r}} Y_{lm}(\hat{\mathbf{r}})^* \psi_n(\mathbf{r})$$

and  $n$  is the index of the Kohn–Sham state,  $Y_{lm}$  is the spherical harmonic function with  $l$  as the angular quantum number and  $m$  as the magnetic quantum number. We consider angular momenta up to  $l = 6$  (I-symmetry). The expansion is made in a

1. CP2K Developers Group (2000–2007), <http://cp2k.berlios.de>.
2. VandeVondele J, et al. (2005) QUICKSTEP: Fast and accurate density functional calculations using a mixed Gaussian and plane waves approach. *Comp Phys Commun* 167:103–128.
3. Goedecker S, Teter M, Hutter J (1996) Separable dual-space Gaussian pseudopotentials. *Phys Rev B* 54:1703–1710.
4. VandeVondele J, Hutter J (2007) Gaussian basis sets for accurate calculations on molecular systems in gas and condensed phases. *J Chem Phys* 127:114105(1–9).

sphere of radius  $R_0$ , where  $R_0$  is chosen based on the radial analysis of atomic shells.

#### Bader Charge Analysis

See [Table S1](#).

#### Electronic Density of States of the Au<sub>102</sub>(p-MBA)<sub>44</sub> Cluster.

See [Fig. S1](#).

**Interaction of p-MBA Molecules with Au Atoms.** Analysis of relaxed fragments, their structures and formation energies leads to a consistent picture of the chemical bonding of the p-MBA ligands as thiolates, i.e., with thiyl RS<sup>•</sup> radicals; see [Figs. S2–S5](#).

5. Perdew JP, Burke K, Ernzerhof M (1996) Generalized gradient approximation made simple. *Phys Rev Lett* 77:3865–3868.
6. Jadzinsky PD, Calero G, Ackerson CJ, Bushnell DA, Kornberg RD (2007) Structure of a thiol monolayer-protected gold nanoparticle at 1.1 Å resolution. *Science* 318:430–433.
7. Blöchl PE (1994) Projector augmented-wave method. *Phys Rev B* 50:17953–17979.
8. Mortensen JJ, Hansen LB, Jacobsen KW (2005) Real-space grid implementation of the projector augmented wave method. *Phys Rev. B* 71:035109(1–11).

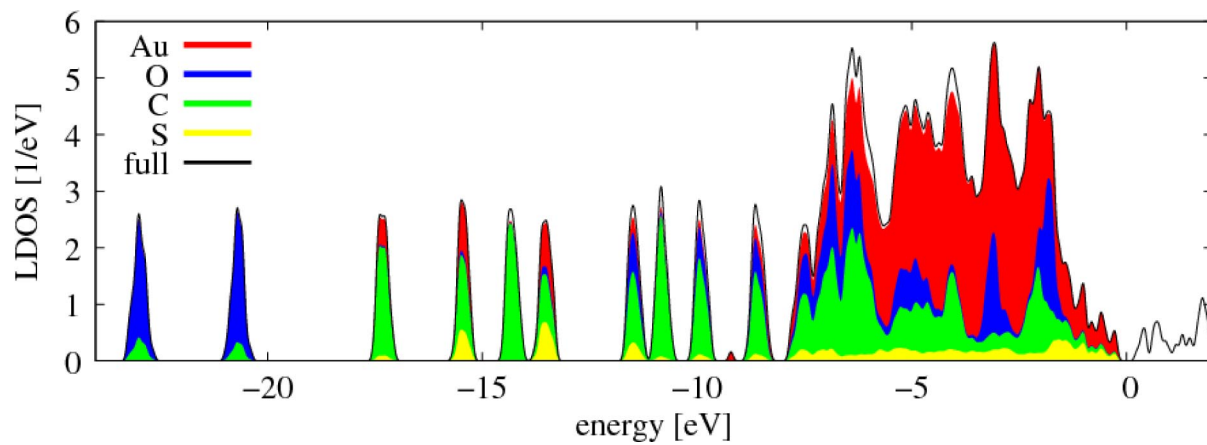


Fig. S1. Element-decomposed electron density of states of the  $\text{Au}_{102}(\text{p-MBA})_{44}$  nanoparticle. The center of the HOMO-LUMO gap is at zero energy.

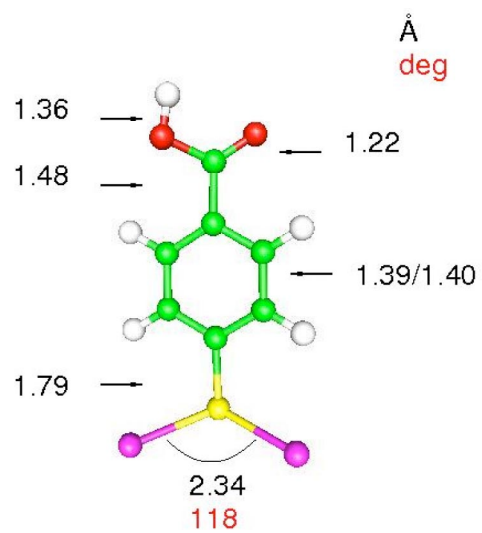


Fig. S2. A single *p*-MBA bridging two Au atoms, formation energy:  $2E(\text{Au}) + E(\text{p-MBA}) - E(\text{p-MBA-Au}_2) = 3.11$  eV

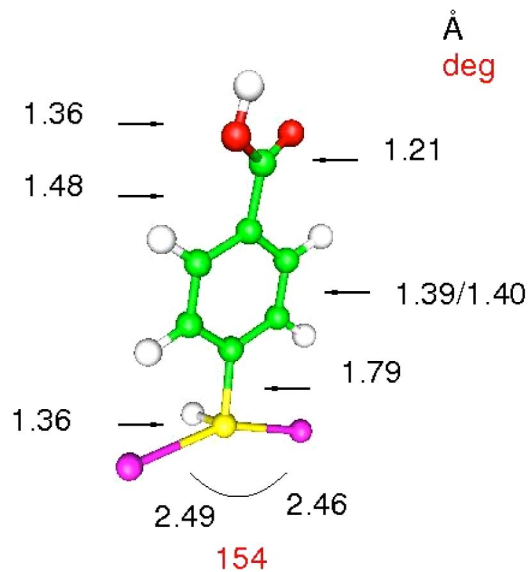


Fig. S3. A single *p*-MBA in thiol form, bridging two Au atoms, formation energy:  $2E(\text{Au}) + E(\text{p-MBA-H}) - E(\text{p-MBA-Au}_2\text{-H}) = 1.62 \text{ eV}$



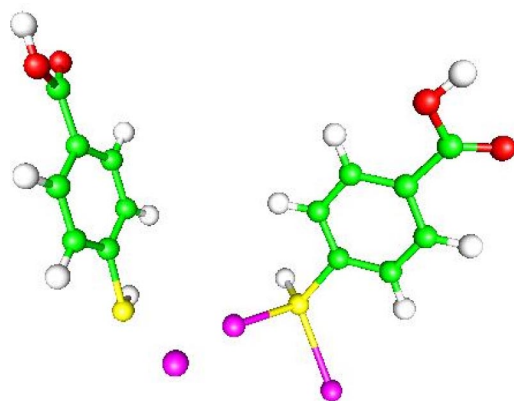


Fig. S5. Same as Fig. S4, but *p*-MBA molecules in thiol form, formation energy:  $3E(\text{Au}) + 2E(\text{p-MBA-H}) - E(\text{p-MBA}_2\text{-Au}_3\text{-H}_2) = 3.62 \text{ eV}$

**Table S1. The total Bader charge for indicated components**

System	Au(core)	Au(ligand)	SR	Cl	PR3
Au <sub>102</sub> ( <i>p</i> -MBA) <sub>44</sub>	+2.21	+3.31	-5.52		
Au <sub>102</sub> (SMe) <sub>44</sub>	+1.30	+0.57	-1.87		
Au <sub>39</sub> (PH <sub>3</sub> ) <sub>14</sub> Cl <sub>6</sub> <sup>-</sup>	-1.92			-3.56	+4.48
Au <sub>11</sub> (PH <sub>3</sub> ) <sub>7</sub> Cl <sub>3</sub>	-0.77			-1.61	+2.38
Au <sub>11</sub> (PH <sub>3</sub> ) <sub>7</sub> (SMe) <sub>3</sub>	-1.33		-0.96		+2.29

For systems 1 and 2 Au(core) means the 79 core atoms. We have employed a publicly available code [Henkelman G, Arnaldsson A, Jonsson H (2006) A fast and robust algorithm for systems 1 and 2 Bader decomposition of charge density. *Comput Mater Sci* 36:354–360; see also <http://theory.cm.utexas.edu/henkelman/research/bader/>].